Ultrafast diagnostics of a plasma generated by an ultrashort, ultraintense laser

PPr901 Project Report

Submitted to

UM-DAE Centre for Excellence in Basic Sciences

Mumbai - 400098, India

in partial fulfilment of the requirements
for the award of the degree of

Integrated M.Sc. (Physics)

by

Varun Joshi

(Roll No. P0201452)

Under the Supervision of

Prof. G Ravindra Kumar
Department of Nuclear and Atomic Physics
TIFR, Mumbai

November, 2024

Certificate

This is to certify that **Varun Joshi** (Roll No.: P0201452) has undertaken his project from 5th June to 30th November, 2024 under the guidance of **Prof. G Ravindra Kumar** at TIFR, Mumbai.

This report titled **"Ultrafast diagnostics of a plasma generated by an ultrashort, ultraintense laser"** is submitted to UM-DAE CEBS, Mumbai towards the institute's academic requirements for the 9th semester (PPr901) of the Int. M.Sc. degree (Physics).
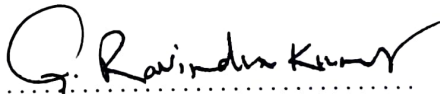
Student Name & Signature

. . . .

Varun Joshi
Roll No.: P0201452

Guide Name & Signature

. . . .

Prof. G Ravindra Kumar
Department of Nuclear and Atomic Physics
TIFR, Mumbai.

Date: 30th November 2024

Declaration

I declare that this written submission represents bona fide work carried out by me under academic guidance. Where others' ideas and words have been included, I have adequately cited and referenced the original source. I declare that I have adhered to all principles of academic honesty and integrity and have not misrepresented or fabricated, or falsified any idea/data/fact/source in my submission.

I understand that any violation of the above will cause disciplinary action by the Institute and can also evoke penal action from the source which has thus not been properly cited or from whom proper permission has not been taken when needed.

. . . .

Varun Joshi
Roll No.: P0201452
Date: 30th November, 2024

Acknowledgements

I take this opportunity to acknowledge and express my gratitude to all those who supported and guided me in the duration of this project.

The biggest thanks goes to my guide, Prof. G Ravindra Kumar (Ravi). He is an exemplary teacher and physicist, and a figure of inspiration. I attended his classes in the previous year and was hooked to his interactive way of teaching, so I decided to write to him to join his lab for this semester. He always emphasizes on looking at problems in the simplest way possible. I can honestly say that I have learnt more in the discussions we had over tea than hours of reading a book or article.

I am fortunate to have interacted with very supportive and welcoming seniors and colleagues at UPHILL lab. I thank Rakeeb, Sagar, Ameya and Dipanjan for their personal and academic help throughout the project. They were kind enough to even let me stay at their rooms some times. Looking at how they help each other in numerous ways- from setting up experiments to heated discussions and constructive criticism, I have learnt how members in a research group can actively collaborate and support each other. I thank Anandam for his simple yet insightful questions and for accompanying me in the occasional stroll to get a coffee. I thank Avani and Dibakar for their constant help as friends and colleagues. I thank Kadam Ji for getting me settled into TIFR.

I also thank my friends Abhay and Adityamani for constantly being in touch and supporting me. At last, I would like to thank my family for their unwavering support and affection.

Varun Joshi

Abstract

The interaction of plasmas with electromagnetic radiation provides a means to understand their various properties. High intensities achieved by focusing light from a coherent source, such as a pulsed *laser* on matter can generate electric fields that exceed the Coulomb field of the nucleus on the electrons, which completely ionizes the material and creates a plasma. To capture the dynamics of the evolving plasma, a replica of the ionizing 'pump' pulse is used to interrogate the plasma at different time delays by measuring changes incurred in it.

The aim of this project was to capture ultrafast dynamics of the freely expanding laser-generated plasma. Two experiments are presented in this light. The first experiment observes the speed of expansion of the plasma surface by Doppler shift measurements using the Pump-Probe technique. Such a measurement gives insights into phenomena such as shocks generated in the plasma.

The second aims to observe the shape evolution of the plasma surface by measuring its wavefront. Instead of a regular pumb-probe measurement, the reflected pump is measured so that a cumulative effect of changes happening only within the duration of the pulse are captured. Wavefront measurements of the reflected pump show what could potentially be a first account of optical signatures of the laser ponderomotive force. The ponderomotive force is a non-linear force that exists due to gradients in electric field. It is an important phenomenon in laser-plasma interaction and plays a role in laser absorption processes and plasma instabilities.

Contents

Contents

List of Figures

Chapter 1

Intense Laser-Matter Interactions: An Introduction

Lasers are devices that produce or amplify electromagnetic radiation in the optical region [Siegman (1986)]. Their coherence, intensity and directionality make them a distinctive source of light. Since their development, lasers have found a wide range of applications in areas ranging from physics, bio-imaging, semiconductor industry to guided weaponry. Short-pulse lasers represent a special class of lasers that are designed to emit intense flashes of light for extremely short durations. A major outcome of compressing energy into short-duration pulses is the ability to reach extremely high intensities. Advances in the development of more and more powerful pulsed lasers, such as the method of Chirped Pulse Amplification (CPA)[Strickland and Mourou (1985)], allow us to routinely reach laser electric fields that exceed, by orders of magnitude, the Coulomb field of nuclei on their electrons!

Evidently, any material that comes in way of such high electric fields gets instantly ionized, making it a plasma. The laser pulse not only produces this plasma, but can also be used to study its interaction with the intense laser field. By recording modifications on a well-described laser pulse, ultrafast dynamics of various fundamental plasma processes can be probed with the laser. From the creation of this plasma, to the mechanisms of energy coupling from the laser field to the plasma, this chapter is a chronological description of events that occur when an ultrashort intense laser falls on matter.

1.1   Atoms in Extreme Light

By compressing a finite amount of energy into a very short pulse duration, ultrafast lasers provide a means to reach extremely high light intensities. Under such extreme light conditions, electrons in the ground state can be lost to ionization. Various mechanisms to reach ionization by intense laser fields have been described in this section. We also learn which mechanism plays more role depending upon the laser parameters.

Multiphoton ionization

Electronic transitions at moderate intensities involve absorption or emission of only one photon with energy corresponding to the energy difference of the two states. Multiphoton ionization is a process in which an atom or a molecule absorbs 2 or more photons simultaneously to move from a lower energy to a higher energy state (or become unbound). This condition for this to happen is that the total energy of the n photons should either match or exceed the energy difference between the states. The rate of ionization (Γ_n) associated with an n photon absorption process is proportional to the light intensity raised to the power n,

$$\Gamma_n = \sigma_n I_L^n \tag{1.1}$$

This, however, is derived from a perturbative approach and breaks down when the laser electric field is comparable or larger than the Coulomb field of the atom.

Tunneling ionization

For a light intensity $\sim 10^{16}$ W/cm^2 the laser electric field reaches close to the atomic field and severely distorts the electric potential experienced by the electron. The distortion happens with every half cycle of the optical pulse, so the electron should tunnel faster than the oscillation of the electric field. Keldysh developed the theory of tunneling ionization by taking the Coulomb potential as a perturbation to the

laser potential. To decide the propensity of this ionization mechanism, he defined a parameter, Γ, which is the ratio of the laser frequency to the tunneling frequency :

$$\Gamma = \frac{\omega}{\omega_{tunnel}} \tag{1.2}$$

It is clear that this mechanism is dominant only when the parameter $\Gamma < 1$. For $\Gamma > 1$, Multiphoton ionization is dominant.
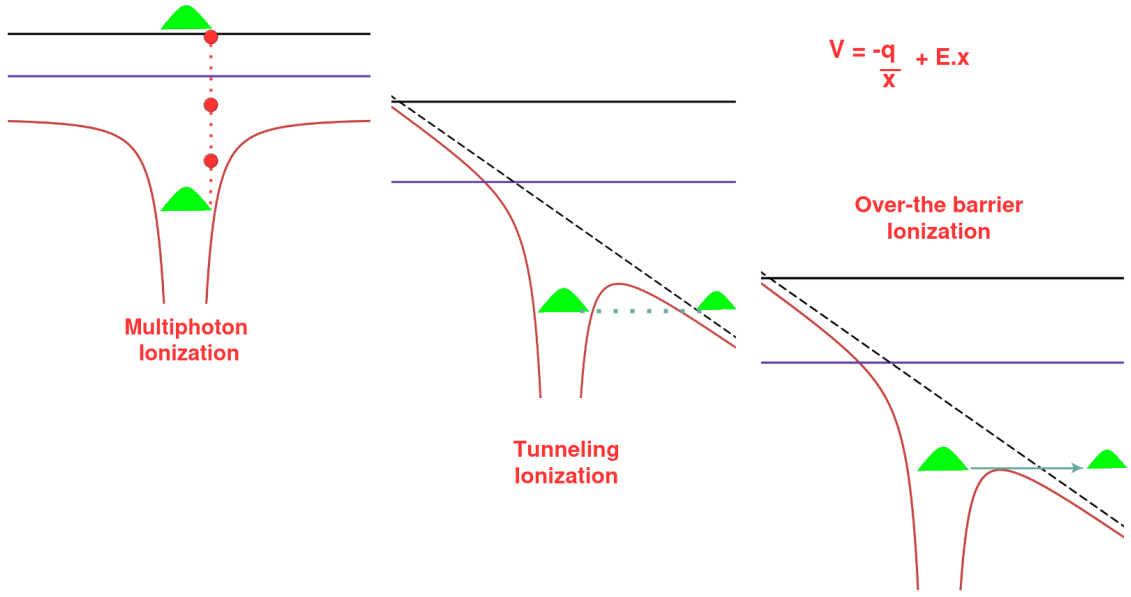
FIGURE 1.1: Mechanisms of ionization in a laser field

Over-the-barrier Ionization

At even higher intensities, the electron is no longer bound by the Coulomb potential and can freely escape. This mechanism is called Over-the-barrier ionization. The threshold can be calculated by equating the distortion of the laser electric field to that of the Coulomb field.

1.2   Extreme light on solids

By mechanisms described in the previous section, the laser frees electrons from the atom. When the laser falls on a solid with a density of the order of 10^{23} /cm^3, this ionization creates a hot-dense plasma. The temporal profile of the pulsed laser, in reality, has a pedestal which is of the order of picoseconds or longer with a femtosecond peak. The picosecond pedestal can be attributed to any residual amplification of spontaneous emission (ASE) in the laser medium during the multiple stages of amplification. So, the femtosecond peak is preceded by a weaker pulse, which is sufficient to ionize the solid (see Fig. 1.2) to form what is called the pre-plasma. In the remaining part of the report, we will describe the interaction in terms of a femtosecond pulse interacting with an inhomogeneous plasma that has a density scale length.

FIGURE 1.2: Contrast of the laser pulse. Courtesy: Sagar Dam

1.3   Ponderomotive force in an optical field

[Eliezer (2002)]

Any real optical field has space-variation and can be described as

$$E(r,t) = E_s(r)\cos\omega t \quad ; \quad B(r,t) = B_s(r)\sin\omega t = -\frac{c}{\omega}\nabla \times E_s(r)\sin\omega t \quad (1.3)$$

An electron in such a field experiences a force which can be written as the following in Gaussian units:

$$m\frac{d\mathbf{v}}{dt} = -e(\mathbf{E_s}\cos\omega t + \frac{v}{c}\times\mathbf{B_s}\sin\omega t) \tag{1.4}$$
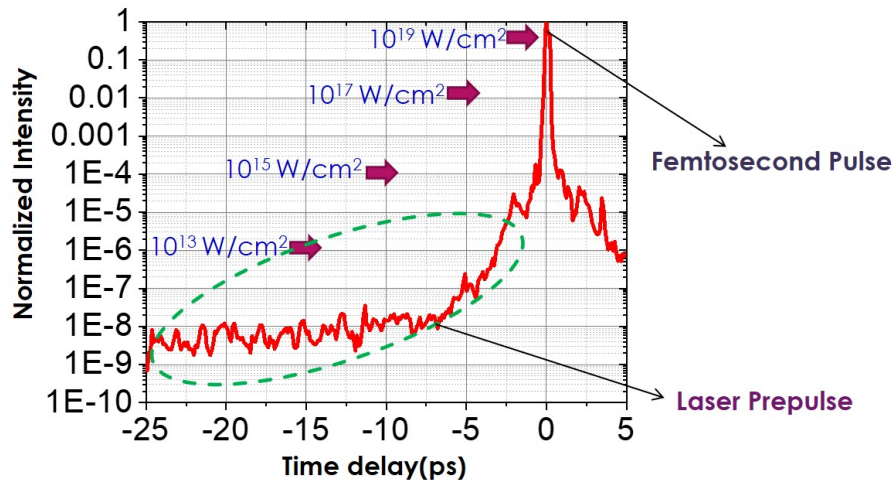
For sufficiently low intensities, the magnetic component can be neglected ($v << c$) and the force equation becomes:

$$m\frac{dv}{dt} = qE_s \quad\Rightarrow\quad v_1 = \frac{eE_s(r_0)}{m\omega}\sin\omega t \quad\Rightarrow\quad v_{max} = \frac{eE_s(r_0)}{m\omega} \tag{1.5}$$

We define a dimensionless parameter a_0

$$a_0 = \frac{v_{max}}{c} = \frac{p}{m_e c} = \frac{eE_s}{m\omega c} \approx 0.855\sqrt{I_{18}\lambda_\mu^2} \tag{1.6}$$

Where I_{18} is the intensity in multiples of 10^{18} W/cm^2 and λ_μ is the wavelength in microns. $a_0 > 1$ corresponds to high intensity and relativistic electrons, in which case (1.4) has to be modified.

For non-relativistic intensities described in (1.5), we have

$$r_1 = \frac{eE_s}{m\omega^2}\cos\omega t \tag{1.7}$$

This is assuming there is no effect of space variation in E_s. When this variation is taken into account, we have

$$E_s = E_S(r_0) + (r_1\cdot\nabla)E_s|_{r=r_0} \quad ; \quad v = v_1 + v_2 \tag{1.8}$$

and the equation of motion for the second term in v is

$$m_e\frac{dv_2}{dt} = -e\left[(r_1\cdot\nabla)E_s(r_0)\cos\omega t + \frac{v_1\times B_s(r_0)\sin\omega t}{c}\right] \tag{1.9}$$

Using 1.5, substituting B from 1.3 and averaging over one optical cycle ($\langle\sin^2\omega t\rangle = \langle\cos^2\omega t\rangle = 1/2$), we get the expression for non-linear force acting on the electron

$$F_{nl} = m_e \left\langle \frac{dv_2}{dt} \right\rangle = \frac{-e^2}{2m_e\omega^2} \left[(E_s \cdot \nabla)E_s + E_s \times (\nabla \times E_s) \right] \tag{1.10}$$

using the identity

$$E_s \times (\nabla \times E_s) = (\nabla E_s) \cdot E_s - (E_s \cdot \nabla E_s)E_s = \frac{1}{2}\nabla \cdot E_s^2 - (E_s \cdot \nabla)E_s$$

the expression for F_{nl} reduces to

$$F_{nl} = \frac{-e^2}{4m_e\omega^2}\nabla E_s^2 \tag{1.11}$$

It is a time averaged non-linear force that exists when there is a spatial gradient in electric field. It acts in the direction opposite to the gradient and is independent of charge sign($\pm$). Electrons and ions move in the same direction in its presence and it is called the **ponderomotive force** (*ponderous*: heavy, *motive*: moving) as it moves the bulk of charges, positive and negative. Relativistic corrections in the derivation of ponderomotive force for high intensities can be found in Mulser and Bauer (2010).

In a plasma with charge density n_e, the ponderomotive force per unit volume is written as

$$f_p = n_e F_{nl} = \frac{-n_e e^2}{4m_e\omega^2}\nabla E_s^2 = \frac{-\omega_{pe}^2}{16\pi\omega^2}\nabla E_s^2 \tag{1.12}$$

where ω_{pe} is the electron plasma frequency described in the next section.

1.4 Laser propagation and absorption mechanisms

[Kruer (2003)]

Plasma with its ability to support waves or collective modes can sustain charge density fluctuations at a characteristic frequency determined by the electrons and/or the ions. There are two such plasma waves: an electron plasma wave of high frequency and an ion acoustic wave of low frequency.

The electron plasma frequency, denoted as ω_{pe}, describes the natural oscillation frequency of electrons in a plasma when displaced from their equilibrium position. Consider an electron plasma with number density n_0 and electrons of mass m_e and charge $-e$. The restoring force on an electron due to a displacement x in a uniform plasma is:

$$F = -eE,$$

where E is the electric field caused by the charge distribution. Using Gauss's law for a uniform charge distribution in Gaussian units, the electric field becomes:

$$E = 4\pi n_0 ex \quad \Rightarrow \quad m_e \frac{d^2x}{dt^2} = -4\pi n_0 ex.$$

Which resembles a simple harmonic oscillator equation, with angular frequency ω_{pe}:

$$\omega_{pe} = \sqrt{\frac{4\pi e^2 n_0}{m_e}} \tag{1.13}$$

When light waves of frequency ω propagate through the plasma, the dispersion relation is given as

$$\omega^2 = \omega_{pe}^2 + k^2 c^2 \tag{1.14}$$

The condition $\omega = \omega_{pe}$ defines a critical plasma density over which the radiation of frequency ω cannot penetrate the plasma. It is expressed as $n_c = 1.1 \times 10^{21}/\lambda_\mu^2$ cm^{-3} where λ_μ is the laser wavelength expressed in microns.

As the pedestal laser couples its energy to the plasma, the plasma grows and develops a radial density gradient. The implication is that light of a certain wavelength can only propagate up to a certain skin depth associated with the corresponding critical density. This radial density gradient gives rise to the most dominant absorption mechanism, known as **resonance absorption**.

When a p-polarized laser pulse is incident at an angle on the pre-plasma, it propagates up to density $n_e = n_c \cos^2\theta$ and some of it reflects (see Fig. 1.3). Critical density corresponds to the surface where the laser oscillation frequency is resonant
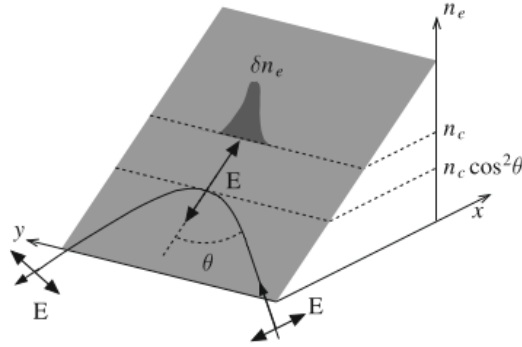
FIGURE 1.3: Resonance absorption of a p-polarized pulse obliquely incident on an inhomogeneous plasma. Taken from Macchi (2013)

with the electron motion in the plasma wave. This resonance enhances the charge density fluctuations at the critical surface and the laser energy couples to the electrons at this surface, which is then diffused into the plasma by collisions and other mechanisms.

When a moving charge gets accelerated due to the presence of other particles and fields, it radiates braking radiation (bremsstrahlung). The inverse of this process happens when a charged particle like electron absorbs light. This process is called "inverse bremsstrahlung" or **collisional absorption**. The absorption fraction of this mechanism increases with the collision frequency (ν_{ie}) and plasma scale length (L). Since ν_{ie} scales as $T^{-3/2}$, this mechanism is not dominant for high intensities ($> 10^{15} \ W/cm^2$) which correspond to high electron temperatures.

Both the mechanisms defined above depend upon pre-plasma scale length and do not play a significant role when the when the laser pulse is extremely clean, so that the scale length is very short ($L << \lambda$) at the arrival of the femtosecond peak. For high intensities, the $v \times B$ term in the force equation cannot be neglected and leads to another laser absorption mechanism known as $\mathbf{J} \times \mathbf{B}$ **heating** [Kruer and Estabrook (1985)].

A linearly polarised light $E = E_0 \hat{y} \sin \omega t$ leads to a longitudinal force

$$f_x = -\frac{m}{4}\frac{\partial v_{osc}^2}{\partial x}(1 - \cos 2\omega t)$$

where the 1st term represents DC ponderomotive force and the second term oscillates with twice the driving laser frequency. This force becomes dominant for relativistic intensities when the quiver velocity, and hence the $v \times B$ term becomes large.

Chapter 2

Experimental Methods

This project deals with the research work aimed at understanding the interaction of an ultrashort ultra-intense laser with solid targets. This chapter is a description of methods and equipment used for the research. The first part describes the TIFR 150 TW laser system along with its pulse characterization methods, followed by a discussion of the experimental techniques used to get results for the experiment. Wavefront measurement of ultrafast laser-generated relativistic plasma is described in the subsequent chapters.

2.1 TIFR Terawatt Laser System

The experiments and results discussed in this thesis were performed at the **U**ltrashort **P**ulse **H**igh **I**ntensity **L**aser **L**aboratory (UPHILL) at TIFR Mumbai which houses a 150 TW (150×10^{12} W) Titanium-doped Sapphire (Ti:Sa) laser with a pulse duration ~ 25 fs and per-pulse energy ~ 3.5 J. The laser uses the **Chirped-Pulse Amplification (CPA)** technique [Strickland and Mourou (1985)] to amplify the energy of a femtosecond seed pulse fed by an **oscillator**. The oscillator is an ultrashort laser in itself. It uses a diode laser to pump a Sapphire crystal heavily doped with Titanium. The crystal has a gain bandwidth, allowing for amplification of a range of frequencies. Out of these, only the modes allowed by the length of the laser cavity are sustained, dictated by boundary conditions. Addition of these allowed modes in

phase, achieved by a process called **mode-locking**, causes them to constructively add in a very short temporal span (see Fig. 2.1), giving an ultrashort pulse. The lower limit of pulse duration is decided by the gain bandwidth of the crystal. Higher gain bandwidth is required for shorter pulses.
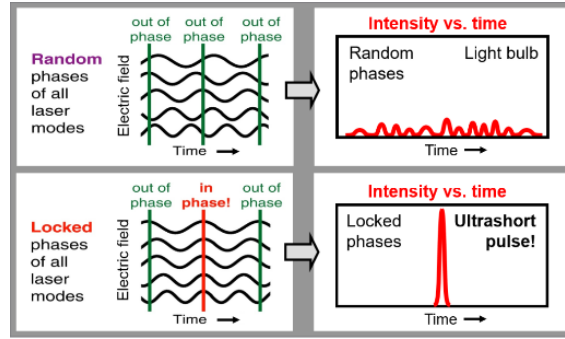

FIGURE 2.1: Mode-locking to produce ultrashort pulses. Courtesy: Rick Trebino

Direct amplification of a femtosecond pulse would lead to damage of the amplifier optics. To amplify it, therefore, it is stretched in time with the help of a pair of gratings that use angular dispersion of the pulse spectrum to create a differential path length and hence relative time delay, called Group Delay Dispersion, for the range of frequencies in the pulse spectrum. The femtosecond pulse gets stretched up to nanoseconds. This nanosecond pulse is amplified from $\sim$nJ through a series of amplification stages to $\sim$J. Temporal stretching of the amplified pulse can be undone by a similar pair of gratings called the compressor, positioned to compensate for the differential path difference created by the stretcher. A schematic of this technique is explained in Fig 2.2.
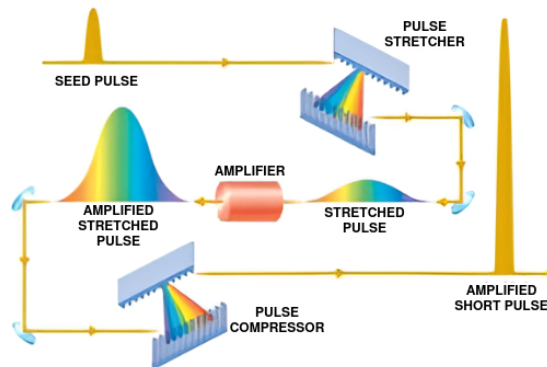

FIGURE 2.2: A schematic of the CPA technique. Taken from Asplund et al. (2019)

2.1.1 Spectrum

The spectrum of the 800 nm laser pulse is shown in Fig 2.3. The spectral bandwidth (FWHM) is ≈ 50 nm and according to the Fourier transform limit (2.1)[Weiner (2009)] for a Gaussian pulse, it can be compressed down to 25-30 fs.

$$\Delta\nu\Delta t \geq 0.44 \tag{2.1}$$
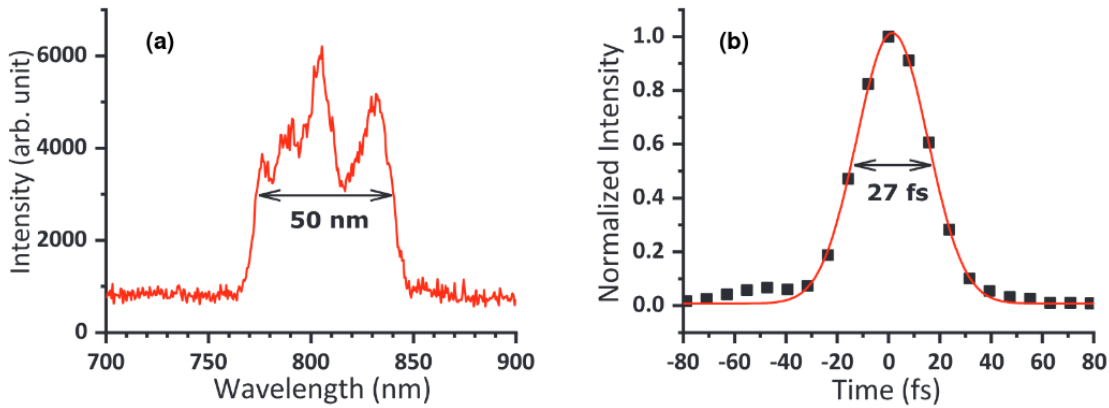
FIGURE 2.3: (a) Spectrum of the 800 nm laser; (b) Pulsewidth measured using SPIDER. Taken from Aparajit et al. (2021)

2.1.2 Pulse characterization

The laser system uses Spectral Phase Interferometry fro Direct Electric Field Reconstruction (SPIDER) [Iaconis and Walmsley (1998)]. In order to measure an ultrashort pulse, SPIDER splits it into two, then shifts the spectrum of one of the replicas by a known amount using nonlinear optics. The pulses are sheared across frequency and give an output spectrum. A phase retrieval algorithm then obtains the temporal profile and phase of the pulse.

2.2   Experimental Setup

After amplification and compression, the beam is routed to the experimental chamber by a series of bending mirrors. From the compressor, the beam line, to the experiment chamber, a vacuum of $\sim 10^{-5}$ mbar is maintained to avoid pulse stretching. For the same reason, a parabolic mirror is used to focus the laser beam onto the target. The incident 8 cm wide beam is focused to a spot of $\approx 7\mu$m (see Fig 2.5). High pulse power confined to a small target area leads to extreme light intensities of the order of 10^{18-19} W/cm^2 required for the experiment.
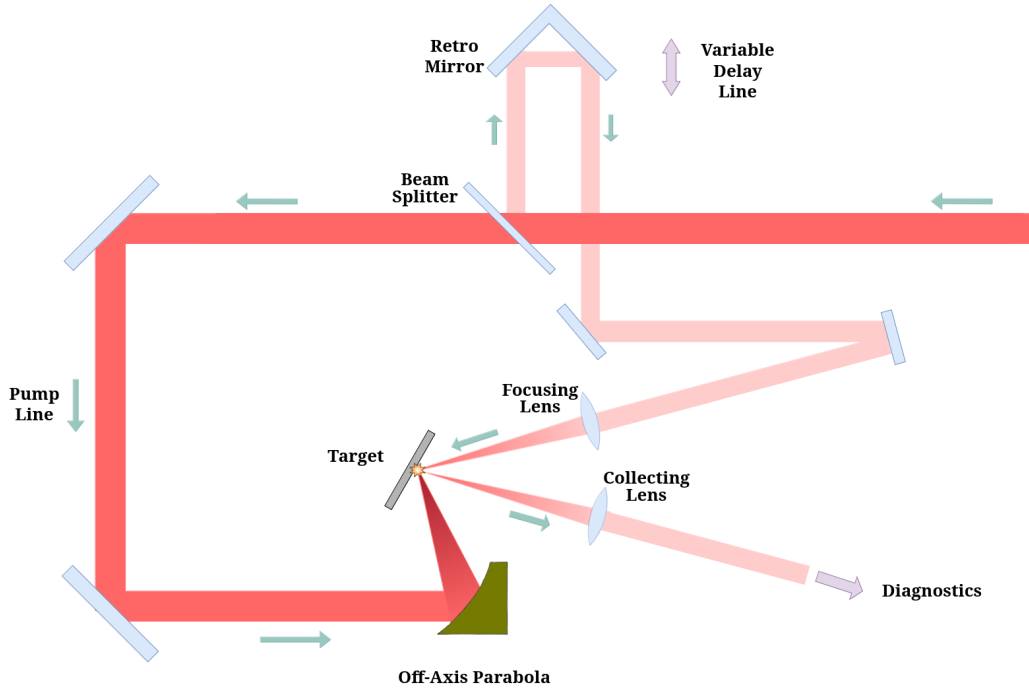
FIGURE 2.4: A schematic of the experimental setup demonstrating the pump-probe technique

After entry into the chamber, a fraction ($\sim 10\%$ energy) of the beam is leaked out of the chamber using a beam splitter, to be used as a probe for measuring properties of the plasma. For this the probe is focused to the same location as the pump and can be given a variable delay on the target with respect to the pump by passing it through a movable retro mirror.

2.3 Diagnostics

2.3.1 Focal Spot Size Imaging

A digital camera is mounted inside the vacuum chamber on the same stage as the target. With a lens of known magnification, it is used to precisely measure the laser focal spot size at low intensities (see Fig. 2.5). It is crucial to measure the spot size as it dictates the light intensity and its effects on the mechanisms of plasma formation and subsequent laser absorption. A precision motorized mount is used to fine tune the x, y orientation and rotation of the parabola to optimize the laser focal spot using feedback from the camera screen.
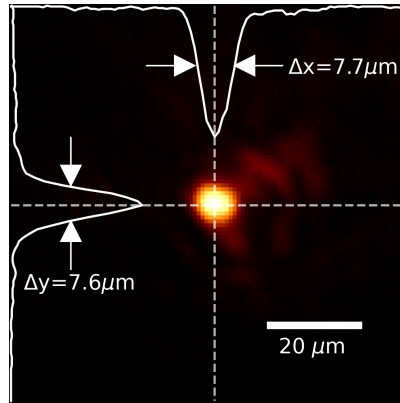
FIGURE 2.5: Imaging of focal spot on a digital camera

2.4 The Pump-Probe Method

In order to capture a process evolving in time, we need another reference event which is at least as brief as the event to be measured. Given that electronic devices respond in the nanosecond timescale, they cannot be used to record events shorter than that. It is clear that an optical measurement is the best shot to achieve such a resolution.

The Pump-Probe method is one such technique (see Fig 2.4). The concept is as follows: A short, intense laser pulse (the "pump") excites a system, initiating a dynamic process, which is the evolution of a plasma in our experiment. A second,

weaker pulse (the "probe") arrives after a controlled time delay to interrogate the system. The measurements are made by recording changes in the probe pulse, such as reflectivity, Doppler shift, polarization and phase changes. Assuming that a phenomenon occurring during the process is changing properties of the probe, its associated quantity can be back-calculated by measuring the reflected probe. The resolution in time is dictated by the duration of the pulse and how precise the delay can be controlled. By varying the time delay between the pump and probe pulses with high precision, a time-resolved "snapshot" of the system's evolution can be recorded, mapping its dynamics on ultrafast timescales.

Although we do not use the pump-probe method explicitly in our main experiment, an understanding of it is nevertheless crucial in understanding the concept of ultrafast measurements.

Space-matching

For the probe to record the changes in the plasma, it has to be focused onto the same location as the pump. This achieved by high precision stages and mounts. The probe path is fixed, but the target stage and parabola are moved to coincide the focal spots of the probe and the pump.

T_0 matching by reflectivity measurement

An optical delay line is used to control the relative delay of the pump with respect to the probe. To do this, we use a retro mirror mounted on a linear stage. Moving the stage by a distance ℓ corresponds to a delay of $2\ell/c$. To give an estimate, a movement of 1 mm would correspond to a time shift of ≈ 6.7 ps.

We need to record the position of the retro mirror that corresponds to zero time delay. To do this we need to employ some property of the plasma which changes dynamically and can be used as a marker of reference time. As an example, let the laser fall on a glass target. We know that the reflectivity of glass is roughly 4%, but after ionization, owing to a surge of free electrons, the plasma becomes metallic in nature. The reflectivity shoots up sharply as the plasma is created,

and then decays as the free electron density reduces because of plasma expansion and electron-ion recombination. We use the pump-probe method to measure the reflectivity as a function of delay and assign our T_0 (or time zero) position to be the one corresponding to the peak in reflectivity (see fig 2.6). Time delays are then assigned with respect to this zero position.
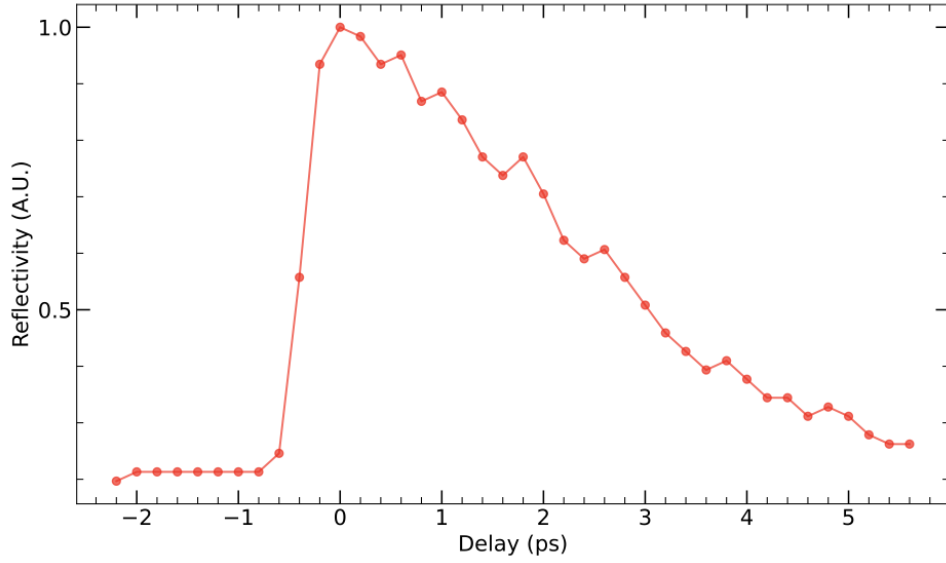

FIGURE 2.6: Reflectivity of glass target as a function of probe delay. T_0 has been taken corresponding to the peak in reflectivity.

Chapter 3

Ultrafast Doppler spectroscopy of laser-generated plasma

3.1 Introduction

The experiments conducted in the duration of this project aim at observing properties of the freely expanding plasma generated by a femtosecond laser. In particular, we try to observe the speed at which the plasma expands, which is the content of this chapter. We use the pump-probe technique described in the previous chapter to record this speed. Measurements are also made to observe the critical surface of plasma, which is discussed in the next chapter.

The interaction of clean femtosecond pulses with solid targets has been studied in the past [Jana et al. (2017, 2019)] where reverse shocks have been observed (Mach No. ~ 2.6). Studies done up to now have only explored the interaction of pulses with contrast 10^{-9} or less. The laser contrast directly affects the pre-plasma scale length, and consequent laser absorption mechanisms.

The experiment described below deals with the interaction of laser pulses with an intensity contrast orders of magnitude higher. A second harmonic crystal, Lithium triborate (LBO) is used to up-convert the laser to 400nm. The intensity conversion depends upon the square of the incident beam intensity ($\propto I^2$), thus the 400nm

laser achieves an extreme contrast (theoretically $\sim 10^{-18}$). The experimental setup to measure Doppler shift is described in the next section.

3.2 Experiment

The pump laser falls on a glass target and creates the plasma. The probe is focused on the location of this plasma and its reflection is collected. The reflection is then split into two- one of the arms is used to determine the T_0 by measurement of reflectivity and the other is routed to a high resolution spectrometer.

To avoid extra wavelengths coming from plasma emission, a BG band pass filter is used before the spectrometer. Reflection from the pump could also be collected in the probe line. To avoid that, the pump beam is passed through a half-wave plate before being focussed on the target. A high extinction polariser is used in the collected probe to ensure that no part of the pump is collected with the probe. The experiment is conducted for various robe delays.

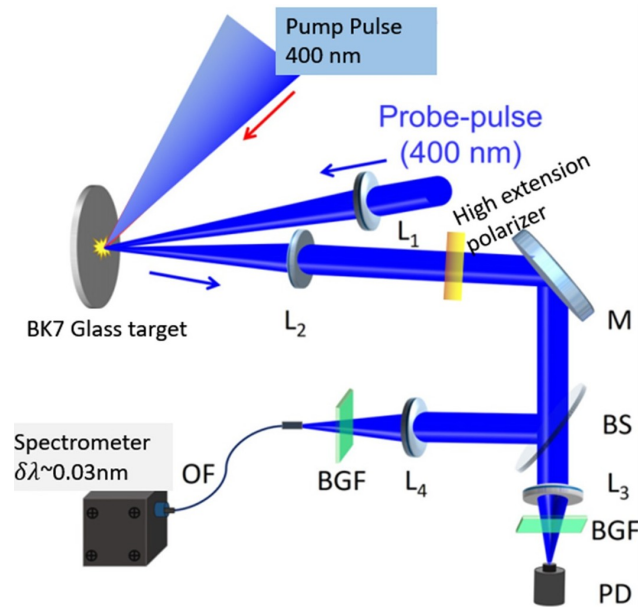FIGURE 3.1: Setup for ultrafast Doppler spectroscopy of expanding plasma. Courtesy: Sagar Dam

The plasma contains free electrons and reflects light like a mirror. It also expands, meaning that there will be a Doppler shift in light reflected from such a mirror which is given by the following formula:

$$\lambda' = \lambda \sqrt{\frac{1-\beta}{1+\beta}} \quad ; \quad \beta = v/c > 1 \tag{3.1}$$

Chapter 4

Wavefront measurement of laser-generated plasma

Any measurement is an act of comparison against a reference. Often enough, we may not have such a reference and we employ a very radical approach, which is to measure against self. An example is the measurement of ultrashort pulses where a shorter reference timescale is not readily available and pulses are characterized by obtaining signals of a replicate pulse smearing across the original pulse [2.1.2]. A similar approach is taken to measure wavefronts using lateral shearing interferometry.

4.1 Lateral Shearing Interferometry

We describe an arbitrary wavefront in terms of its deviation from a flat plane, expressed as wavefront error function $W(x, y)$ whose value varies laterally across the surface. We take a replica of this wavefront and laterally shear it with some distance S. Constructive interference happens between the two for loci described by
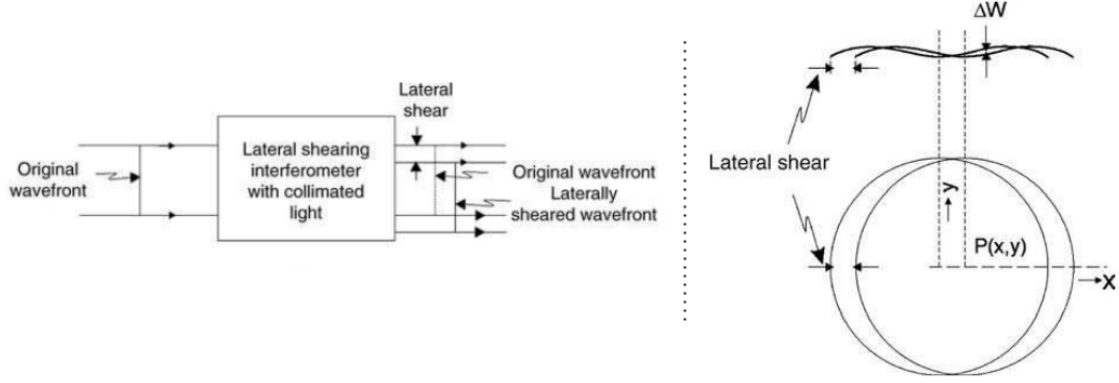
$$\Delta W(x, y) = n\lambda$$

FIGURE 4.1: Lateral Shearing Interferometry. Wavefront is reconstructed by measuring changes in wavefront error (ΔW) with lateral shear. Taken from Strojnik et al. (2007)

Suppose the replica is sheared by an arbitrarily small distance, then we can rewrite the equation as:

$$\frac{\partial W(x,y)}{\partial x} S = n\lambda \tag{4.1}$$

$\frac{\partial W}{\partial x}$, found by interferometry, can give information of the wavefront error function, which describes its shape. In the sections that follow, we describe a mechanism which provides a means to have such a lateral shearing.

4.2 The Hartmann Mask as a lateral shearing interferometer

In 1900, Hartmann proposed a simple method for testing of optical components, that uses a mask of holes periodically arranged on a grid. The holes divide the incoming light into smaller beams which are deflected from the normal according to local tilts in the wavefront (see Fig. 4.2(a)).

This section describes the theoretical foundation of the classical Hartmann mask. For simplicity, a 1-dimensional explanation is given.
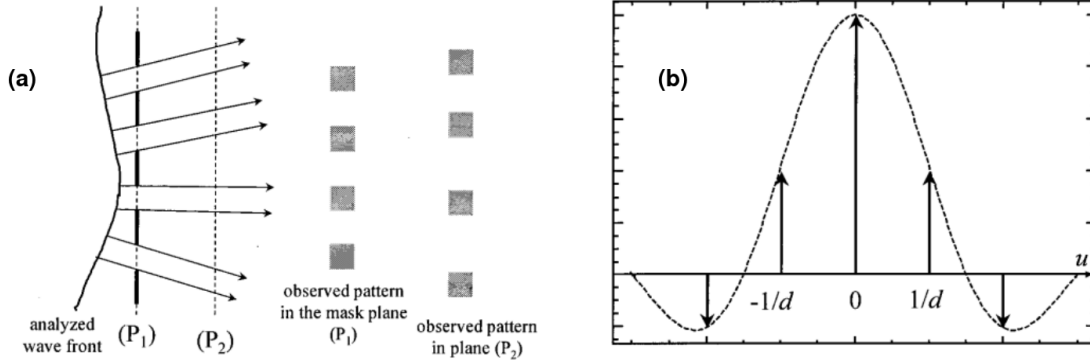
FIGURE 4.2: (a) Principle of the Hartmann mask. P_1 is the plane of the mask, P_2 is a certain distance ahead of it. (b) Diffraction orders in a sinc envelope. Taken from Primot and Guérineau (2000)

Transmittance from periodic array of apertures with pitch 'd' and size 'a' can be written as

$$t(x) = \Pi_a(x) * comb_d(x) \tag{4.2}$$

where Π_a is a rectangular function of width a (=1 in $[-a/2 , a/2]$ and 0 elsewhere) and $comb_d(x)$ is a comb of Dirac delta functions spaced d distance apart.

Amplitudes of the diffraction orders is given by a Fourier transform

$$FT(u) = \frac{\sin \pi ua}{\pi ua} comb_{1/d}(u) \tag{4.3}$$

The pitch and hole size can be manipulated such that the sinc function in (4.3) decreases fast and only orders 0 and ± 1 are significant, so that the transmittance from the mask can be approximated as a sum of these orders:

$$t(x) = C_o + C_1 \exp\left(2i\pi x/d\right) + C_{-1} \exp\left(-2i\pi x/d\right) \tag{4.4}$$

where C_i are the amplitudes of the respective diffraction orders. The zeroth order propagates along the normal of the mask plane. The orders ± 1 are phase delayed and propagate at angles $\pm\lambda/d$ with respect to it. At multiples of a certain distance, called the Talbot distance, the phase delay is equal to $2n\pi$ and the diffracted orders are also laterally shifted (see Fig 4.3).
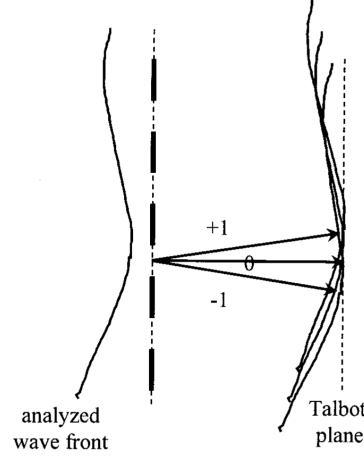
FIGURE 4.3: Hartmann test as a lateral shearing interferometer. The pattern corresponds to three replicas of the incident wavefront that constructively interfere at the Talbot distance. Taken from Primot and Guérineau (2000)

The phase acquired for an optical path length $g(x)$ is given as $E_i = \exp\left(2\pi i g(x)/\lambda\right)$. To arrive at the interferogram $I(x, z)$ at a distance z from the mask, we first write the scalar electric field by the three orders of an arbitrary wavefront diffracted from the Hartmann mask:

$$E(x, z) = \sum_{p=0,\pm 1} C_p \exp\left[\frac{2\pi i}{\lambda}(x\sin\theta_p + z\cos\theta_p) + g(x - z\tan\theta_p)\right] \qquad (4.5)$$

Where the second term accounts for the shape of the wavefront. Here $\theta_p = \sin^{-1}(\lambda p/d)$. $I(x, z) = EE^*$ and it simplifies to the following:

$$I(x, z) = M_0 + M_1 \cos\left[\frac{2\pi}{d}\left(x - z\frac{dg}{dx}\right)\right] + M_2 \cos\left[\frac{4\pi}{d}\left(x - z\frac{dg}{dx}\right)\right] \qquad (4.6)$$

where $M_0 = C_0^2 + 2C_1^2$; $M_1 = 4C_0C_1\cos\left(\pi\lambda z/d^2\right)$; $M_2 = 2C_1^2$
The first term is a constant and of no pertinence in reconstructing the wavefront. The other two terms can be viewed as a frequency modulation of a carrier cosine wave of frequency $2\pi/d$ with a factor proportional to the product of transverse wavefront slope times a magnification factor of z. A numerical demodulation will give the derivative of the wavefront error.

Contrast of the second term varies cosinusoidally along z with a period of d^2/λ. For monochromatic light, this contrast degrades heavily at regular intervals, and the

interferogram has to be obtained in the vicinity of Talbot planes. For polychromatic light, visibility of self-images decreases with z and the interferogram can only be analyzed in close vicinity of the mask. Due to these shortcomings, the regular Hartmann mask has a limited scope for use.

4.3   The Modified Hartmann Mask (MHM)

Primot and Guérineau (2000) suggested a modification to the Hartmann mask to improve its versatility. They proposed complementing the mask with a phase chessboard (see Fig. 4.4). The pitch of this chessboard is twice that of the mask, and it has a depth corresponding to a phase difference of π for a particular wavelength. Thus, alternate square apertures have π phase difference with respect to each other.
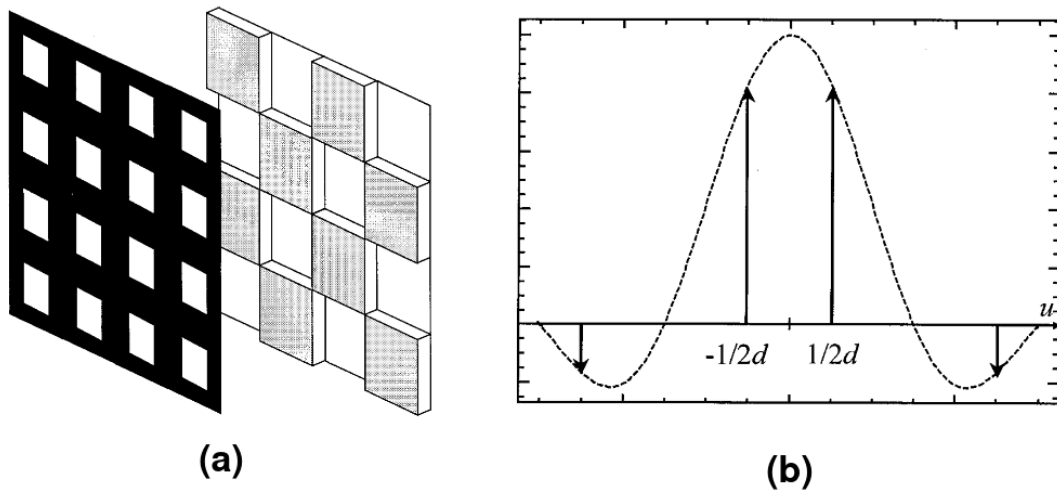

FIGURE 4.4: (a) Hartmann mask with with addition of a phase chessboard. (b) Diffraction orders for MHM for $a = 2d/3$. The two central orders store the maximum energy Look at 4.2(b) for comparison. Taken from Primot and Guérineau (2000)

Transmission from this modified Hartmann mask is written as

$$tp(x) = \Pi_a(x) * [comb_d(x) \exp(i\pi x/d)] \tag{4.7}$$

where the exponential models the alternating phase. The amplitudes of diffracted orders are:

$$FT_p(u) = \frac{\sin(\pi ua)}{\pi ua}[comb_{1/d}(u) * \delta(u - 1/2d)] \tag{4.8}$$

Which means that the orders have been shifted by $1/2d$ and there are two prominent diffraction orders at angles $\pm\lambda/2d$ (see Fig 4.4(b)). The pitch and aperture size are set such that $(a = 2d/3)$ most of the energy is contained in these two orders and the transmission can be approximated as:

$$tp(x) = C_{1/2}\exp\left(i\pi x/d\right) + C_{-1/2}\exp\left(-i\pi x/d\right) \tag{4.9}$$

Here $C_{1/2} = C_{-1/2}$ and the interferogram for a general aberrant wavefront comes out as follows:

$$tp(x, z) = 2C_{1/2}^2\left[1 + \cos\left[\frac{2\pi}{d}\left(x - z\frac{dg}{dx}\right)\right]\right] \tag{4.10}$$

A comparison with 4.6 shows that the contrast is propagation invariant. As there is no wavelength dependence, it is also achromatic, and therefore, the limitations of a regular Hartmann mask are overcome by the MHM. This 1-dimensional explanation shows the use of two diffraction orders interfering to provide a means of lateral shearing. In a 2-dimensional description, this involves 4 orders and the arrangement is called a Quadri-Wave Lateral Shearing interferometer (QWLSI). Chanteloup (2005) gives a detailed description of the QWLSI.

UPHILL lab uses an SID4 wavefront sensor that uses the phase chessboard. For 800 nm wavelength, it has a resolution of 5nm in optical path difference. Initially used as a feedback system for adaptive optics in the laser system, it is now being used for phase measurement experiments.

4.4 Experiment

As previously discussed, the time resolution of the Pump-Probe technique depends upon the duration of the pulse. The probe is a weak beam and it is hard to align optics with a weak 800 nm (close to IR) beam which is not easy to see. For this reason, in most of our pump-probe diagnostics, we up-convert the beam to 400 nm (blue) which is easier to align. This, however reduces the bandwidth and consequently stretches the pulse in time. In our setup for pump-probe diagnostics (see Fig 2.4), we use a convex lens to focus the probe on the target, just because it is easier to focus a beam with it. The probe also has to pass through a glass window to fall on a retro mirror which is located outside the vacuum mirror because of space constraints. Due to these additional transmissive optics and second harmonic conversion, the probe pulse stretches to about 200 fs before it is incident on the plasma and cannot be used for ultrafast diagnostics at smaller timescales.

For this reason, we use a much simpler setup with the pump having a dual role-both as the pump and the probe. The pump pulse comes and excites the target. A part of this pulse goes into creating and exciting the plasma. The beam is not entirely absorbed and the reflected part captures modifications introduced by the laser-generated plasma. We measure the wavefront of this reflected pump with the SID4 wavefront sensor so as to observe changes in as short a time scale as the pulse width itself. Fig 4.5 describes the experimental setup.
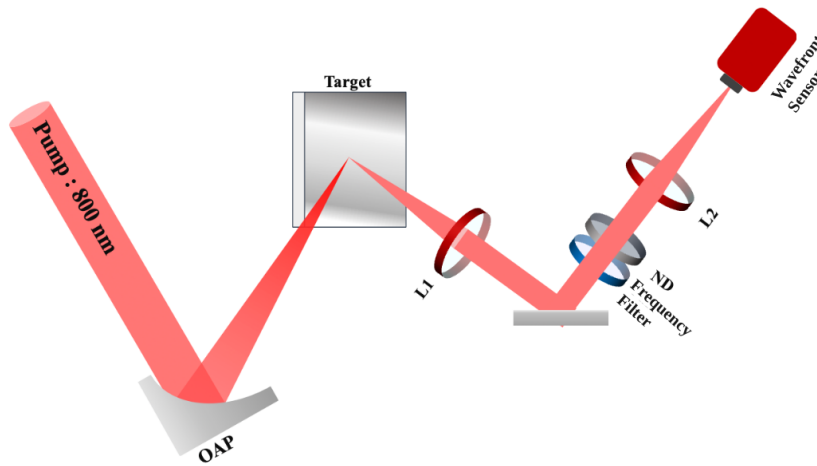

FIGURE 4.5: Setup for the wavefront measurement in pump reflection geometry. Courtesy: Sk Rakeeb

Before collection into the wavefront sensor, the reflected pump is passed through a filter to exclude extra frequencies coming from the plasma and a neutral density filter to suitably attenuate the signal.

The experiment is run for different laser intensities. Phase plots for each run are analysed using python (see Fig. 4.6). The line-cut for optical path difference is an estimate of the curvature in critical density surface, from which the reflection happens, and is therefore an estimate of the laser ponderomotive force.
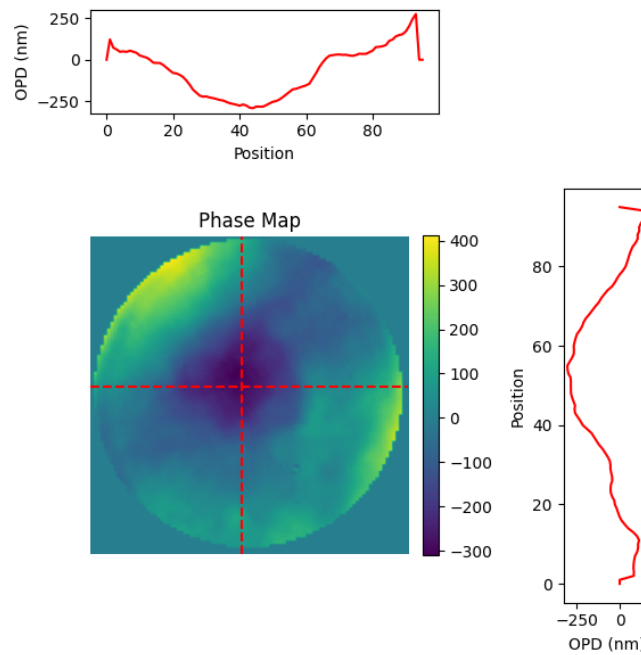

FIGURE 4.6: Result of phase measurement. Phase difference is converted to optical path difference for 800 nm

Chapter 5

Results and Conclusions

5.1 Doppler shift of expanding plasma

Data is presented for two different intensities. A Gaussian fit is done to analyse the spectrum for each shot. To get a reading for different time delays, the laser is set to shoot at 10 Hz while the retro mirror moves to change the delay. Each obtained shot corresponds to a different delay.
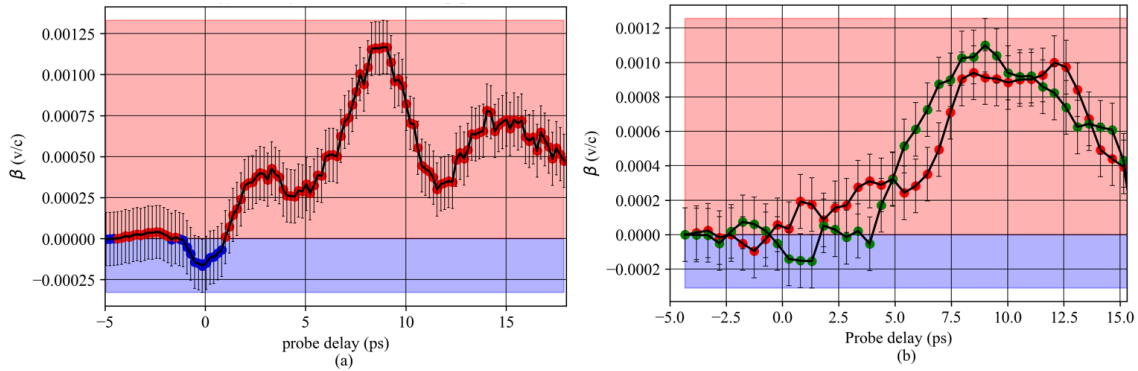

FIGURE 5.1: Time varying Doppler shift of expanding plasma for (a) $I = 3 \times 10^{17}$ W/cm^2 and (b) $I = 1.3 \times 10^{18}$ W/cm^2. [In preparation: Sagar Dam et al]

For a negative probe delay, we do not expect β to be anything other than 0, because there is no plasma and the reflection happens from a static glass surface. For a positive delay, the reflection is captured from a moving plasma surface and we should observe changes for different positive probe delays if the speed of expansion changes.

A somewhat oscillatory behaviour is observed for $I = 3 \times 10^{17}$ W/cm². For a probe delay close to 0, a negative trend is observed in β, although much can't be commented on it seeing that the trend lies within the error bar.

The trend for a different intensity $I = 1.3 \times 10^{18}$ W/cm² looks completely different. The second graph has 2 plots for 2 different runs of the experiment. β is close to 0 for delays up to $\sim 5ps$ but then grows and reaches a maximum at ~ 10 ps, after which it falls again.

Changes in the trends are expected to be a consequence of the laser a_0 deciding which phenomenon occurs with more propensity. A collaboration is ongoing with a theory and simulation group to understand and draw parallels between theory, simulations and results obtained in the experiments.

5.2 Critical surface curvature at different intensities

The experiment is done for different peak intensities and the results are described in the plot that follows.
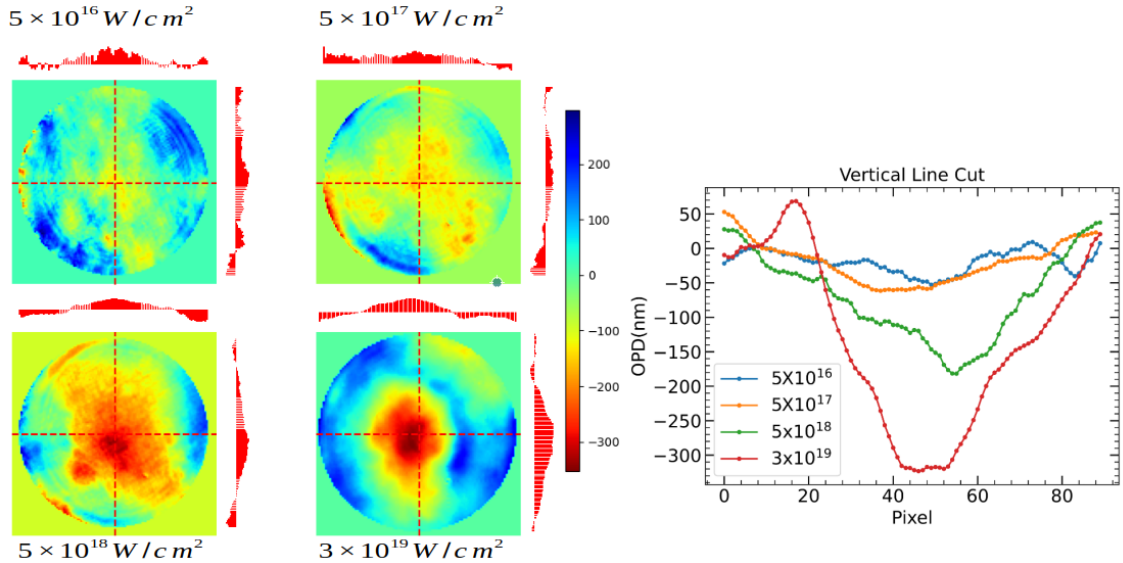

FIGURE 5.2: Phase plots and corresponding line cuts for curvature of critical density surface at different laser intensities (in W/cm^2). [In preparation: Sk Rakeeb et al]

The curvature of critical density surface is radially inwards and reaches as much as half the laser wavelength for the highest intensity ($a_0 \approx 3.75$) used in the experiment. Evidently more curvature is seen for higher intensities.

What is interesting to note is that this inward curvature is only seen in the pump reflection geometry. The results for pump-probe geometry, which are at a longer timescale, only show a plasma expanding freely outwards. This means that the phenomenon responsible for the inward curvature has to be as short-lived as the laser pulse width. Since the ponderomotive force ($\sim \nabla E^2$) lasts only for the pulse duration, the experiment is most likely an optical measurement of this phenomenon. Other potential mechanisms involving the movement of ions etc occur at a larger timescale ($>$ ps) owing to large ion mass.

There is an ongoing collaboration with a different theory and simulation group to look for similarities between what is expected from simulations and what is observed experimentally. A thorough and complete explanation of the results is yet to be made.

5.3 Future prospects for wavefront measurement

Various modifications can be made on the pulse which would also serve as a test of our claim. They have been describe below:
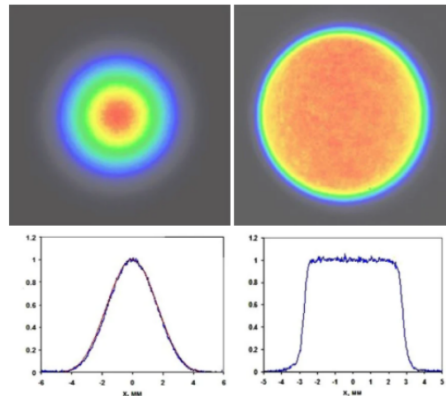

FIGURE 5.3: Shaping of transverse beam profile at focus with a beam homogenizer. Left (Gaussian) and Right (Top-Hat). Taken from Edmund Optics website

1. Temporal shaping of the beam will change the longitudinal intensity profile of the beam as it falls on the target, modifying its longitudinal field gradient.

2. To shape the intensity/field profile in the transverse direction, a specialized optic known as a beam homogenizer can be used.

3. Laser absorption mechanisms crucially depend upon the scale length. By using a second harmonic (400nm) conversion crystal whose conversion depends upon I^2, a pulse with a weaker pre-pulse can be obtained, so that the plasma is only created immediately before the arrival of the femtosecond peak and the pre-plasma scale length is short.

All of these modifications are planned for future experiments at UPHILL, TIFR.

[NOTE:] Images used in this report are either created by me or sourced from the respective authors who have been appropriately cited. Use of images from the experimental results presented in the report without permission of the authors is prohibited.

References

Aparajit, C., Jana, K., Lad, A.D., Ved, Y.M., Couairon, A., Kumar, G.R., 2021. Efficient second-harmonic generation of a high-energy, femtosecond laser pulse in a lithium triborate crystal. Opt. Lett. 46, 3540–3543. URL: https://opg.optica.org/ol/abstract.cfm?URI=ol-46-15-3540, doi:10.1364/OL.423725.

Asplund, M.C., Johnson, J.A., Patterson, J.E., 2019. The 2018 nobel prize in physics: Optical tweezers and chirped pulse amplification. Analytical and Bioanalytical Chemistry 411, 5001–5005. URL: https://doi.org/10.1007/s00216-019-01913-z.

Chanteloup, J.C., 2005. Multiple-wave lateral shearing interferometry for wave-front sensing. Applied Optics 44, 1559. URL: https://opg.optica.org/abstract.cfm?URI=ao-44-9-1559, doi:10.1364/AO.44.001559.

Eliezer, S., 2002. The Interaction of High-Power Lasers with Plasmas. CRC Press, Boca Raton. doi:10.1201/9781420033380.

Iaconis, C., Walmsley, I.A., 1998. Spectral phase interferometry for direct electric-field reconstruction of ultrashort optical pulses. Optics Letters 23, 792–794. URL: https://opg.optica.org/ol/abstract.cfm?uri=ol-23-10-792, doi:10.1364/OL.23.000792. publisher: Optica Publishing Group.

Jana, K., Blackman, D.R., Shaikh, M., Lad, A.D., Sarkar, D., Dey, I., Robinson, A.P.L., Pasley, J., Ravindra Kumar, G., 2017. Probing ultrafast dynamics of solid-density plasma generated by high-contrast intense laser pulses. Physics of Plasmas 25, 013102. URL: https://doi.org/10.1063/1.5005176, doi:10.1063/1.5005176.

Jana, K., Lad, A.D., Shaikh, M., Kumar, V.R., Sarkar, D., Ved, Y.M., Pasley, J., Robinson, A.P.L., Kumar, G.R., 2019. Generation of a strong reverse shock wave in the interaction of a high-contrast high-intensity femtosecond laser pulse with a silicon target. Applied Physics Letters 114, 254103. URL: https://doi.org/10.1063/1.5097918, doi:10.1063/1.5097918.

Kruer, W., 2003. The Physics of Laser Plasma Interactions. Frontiers in Physics, CRC Press. URL: https://www.taylorfrancis.com/books/mono/10.1201/9781003003243/physics-laser-plasma-interactions-william-kruer, doi:10.1201/9781003003243.

Kruer, W.L., Estabrook, K., 1985. J×b heating by very intense laser light. The Physics of Fluids 28, 430–432. URL: https://doi.org/10.1063/1.865171, doi:10.1063/1.865171.

Macchi, A., 2013. Electron Acceleration. Springer Netherlands, Dordrecht. pp. 59–79. URL: https://doi.org/10.1007/978-94-007-6125-4_4, doi:10.1007/978-94-007-6125-4_4.

Mulser, P., Bauer, D., 2010. The Ponderomotive Force and Nonresonant Effects. Springer Berlin Heidelberg, Berlin, Heidelberg. pp. 193–227. URL: https://doi.org/10.1007/978-3-540-46065-7_5, doi:10.1007/978-3-540-46065-7_5.

Primot, J., Guérineau, N., 2000. Extended Hartmann test based on the pseudoguiding property of a Hartmann mask completed by a phase chessboard. Applied Optics 39, 5715–5720. URL: https://opg.optica.org/ao/abstract.cfm?uri=ao-39-31-5715, doi:10.1364/AO.39.005715. publisher: Optica Publishing Group.

Siegman, A.E., 1986. Lasers. University Science Books.

Strickland, D., Mourou, G., 1985. Compression of amplified chirped optical pulses. Optics Communications 56, 219–221. URL: https://www.sciencedirect.com/science/article/pii/0030401885901208, doi:https://doi.org/10.1016/0030-4018(85)90120-8.

Strojnik, M., Paez, G., Mantravadi, M., 2007. Lateral Shear Interferometers. John Wiley Sons, Ltd. chapter 4. pp. 122–184. URL: https://onlinelibrary.wiley.com/doi/abs/10.1002/

9780470135976.ch4, doi:https://doi.org/10.1002/9780470135976.ch4, arXiv:https://onlinelibrary.wiley.com/doi/pdf/10.1002/9780470135976.ch4.

Weiner, A.M., 2009. Ultrafast-Pulse Measurement Methods. John Wiley Sons, Ltd. chapter 3. pp. 85–146. URL: https://onlinelibrary.wiley.com/doi/abs/10.1002/9780470473467.ch3.